iScience

CellPress
OPEN ACCESS

Article

RUVBL1 accelerates tongue squamous cell carcinoma by mediating CRaf/MEK/ERK pathway

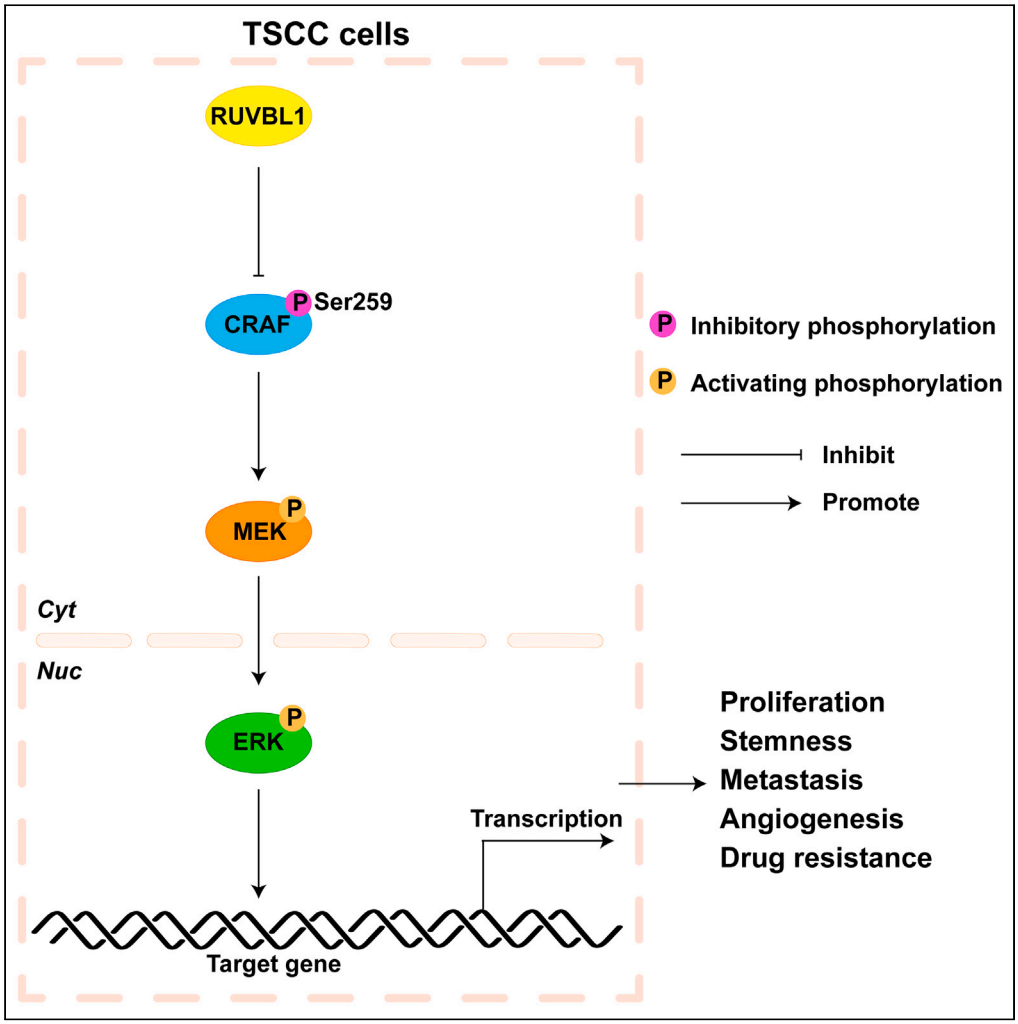

Xin-yu Zhang, Yang Liu, Qiong Rong, Ming-yue Qi, Hui Guo

guohuiggxx@163.com

Highlights

RUVBL1 facilitates TSCC proliferation, stemness, metastasis, and angiogenesis *in vitro*

RUVBL1 accelerates the malignant process of TSCC *in vivo*

CRAF/MEK/ERK signaling is a downstream target of RUVBL1

Zhang et al., iScience *27*, 109434
April 19, 2024
https://doi.org/10.1016/j.isci.2024.109434

iScience

CellPress
OPEN ACCESS

Article

RUVBL1 accelerates tongue squamous cell carcinoma by mediating CRaf/MEK/ERK pathway

Xin-yu Zhang,[1,3] Yang Liu,[2,3] Qiong Rong,[1] Ming-yue Qi,[2] and Hui Guo[1,4,*]

SUMMARY

RAF/MEK/ERK pathway is frequently activated in tumor. Therefore, this study will investigate the function of RUVBL1 (RAF-binding protein) in tongue squamous cell carcinoma (TSCC). Bioinformatics was performed to identify differentially expressed mRNAs (DE-mRNAs) in TCGA-oral squamous cell carcinoma, GSE13601, and GSE34105 datasets. A total of 672 shared DE-mRNAs were identified in three datasets, and they are regulating metastasis and angiogenesis. Patients with RUVBL1 low expression had high overall survival. Overexpressing RUVBL1 enhanced the viability, wound healing percentage, invasion, sphere formation, angiogenesis, and resistance to cisplatin and 5-fluorouracil in CAL-27 and SCC-4 cells, and the opposite results were obtained by knocking down RUVBL1. Moreover, overexpression of RUVBL1 bolstered tumor growth *in vivo*. Strikingly, RUVBL1 diminished the phosphorylation of CRAF Ser259, which led to activation of the MEK/ERK pathway. In conclusion, RUVBL1 contributes to the malignant biological behavior of TSCC via activating the CRAF/MEK/ERK pathway. This provides molecular mechanisms and perspectives for targeted therapy of the CRAF/MEK/ERK pathway.

INTRODUCTION

Head and neck squamous cell carcinoma (HNSCC) frequently occurs in the paranasal sinus, oral cavity, oropharynx, hypopharynx, and the mucous membranes of the larynx and is the sixth largest malignant tumor in the world.[1] Tongue squamous cell carcinoma (TSCC) is one of the malignant tumors of HNSCC, accounting for 38% of HNSCC and 90% of oral squamous cell carcinoma.[1–3] Tobacco, betel, alcohol, poor oral hygiene, and human papillomavirus infection are risk factors for the development of TSCC.[4,5] According to statistics, there are approximately 405,000 new cases of TSCC worldwide each year, and the patient survival rates at two and five years after surgery are 40.6% and 31.2%, respectively.[3,6,7] Therefore, there is an urgent need to understand and improve the molecular mechanisms associated with the development of TSCC and to develop targets, which is of great significance for improving the efficacy of targeted therapy for TSCC.

Currently, the clinical implementation of the TSCC treatment is based on surgical treatment with adjunctive postoperative radiotherapy. The first-line drug strategy for TSCC treatment is the epidermal growth factor receptor (EGFR)-targeting inhibitor cetuximab in combination with cisplatin (DDP) and 5-fluorouracil (5-FU).[8,9] This therapeutic strategy improves the survival of some patients to some extent. Nevertheless, the EGFR gene is characterized by high mutation, resulting in limiting therapeutic efficacy of TSCC and the exhibition of drug resistance and serious adverse effects such as rash and paronychia.[8,10] Notably, the RAF Proto-Oncogene, Serine/Threonine-Protein Kinase (RAF)/mitogen-activated extracellular signal-regulated kinase (MEK)/extracellular signal-regulated kinase (ERK) is a critical downstream pathway for functioning of EGFR-targeted inhibitors.[11,12] RAF/MEK/ERK belongs to the mitogen-activated protein kinase (MAPK) signaling pathway, which plays an important role in cell proliferation, apoptosis, motility, and metabolism.[13,14] RAF belongs to the serine/threonine kinases and has three subtypes in mammals, ARAF, BRAF, and CRAF. Current studies have confirmed that BRAF is closely associated with the development of many kinds of tumors, especially melanoma, while ARAF and CRAF, especially ARAF, have been rarely reported.[13,14] It is well known that phosphorylation of RAF leads to activation of the downstream MEK/ERK pathway, which accelerates the malignant biological behavior of tumors, including TSCC. Therefore, understanding the regulatory mechanisms associated with the RAF/MEK/ERK pathway provides perspectives for targeted chemotherapeutic regimens and development of targets for TSCC.

In this study, we proposed to analyze the correlation between RUVBL1, a CRAF-binding protein we previously identified,[15] and the prognosis of TSCC patients using bioinformatics, and to explore the effects of RUVBL1 on the malignant biological behaviors of TSCC *in vivo* and *in vitro*. This study aims to refine the molecular mechanisms associated with the RAF/MEK/ERK pathway in TSCC, and to provide an abundant experimental basis for the development of future strategies involving RUVBL1 as a chemotherapeutic target in TSCC.

[1]The First People's Hospital of Yunnan Province, Affiliated Hospital of Kunming University of Science and Technology, Kunming, Yunnan Province 650032, China
[2]Kunming University of Science and Technology, Kunming, Yunnan Province 650500, China
[3]These authors contributed equally
[4]Lead contact
*Correspondence: guohuiggxx@163.com
https://doi.org/10.1016/j.isci.2024.109434

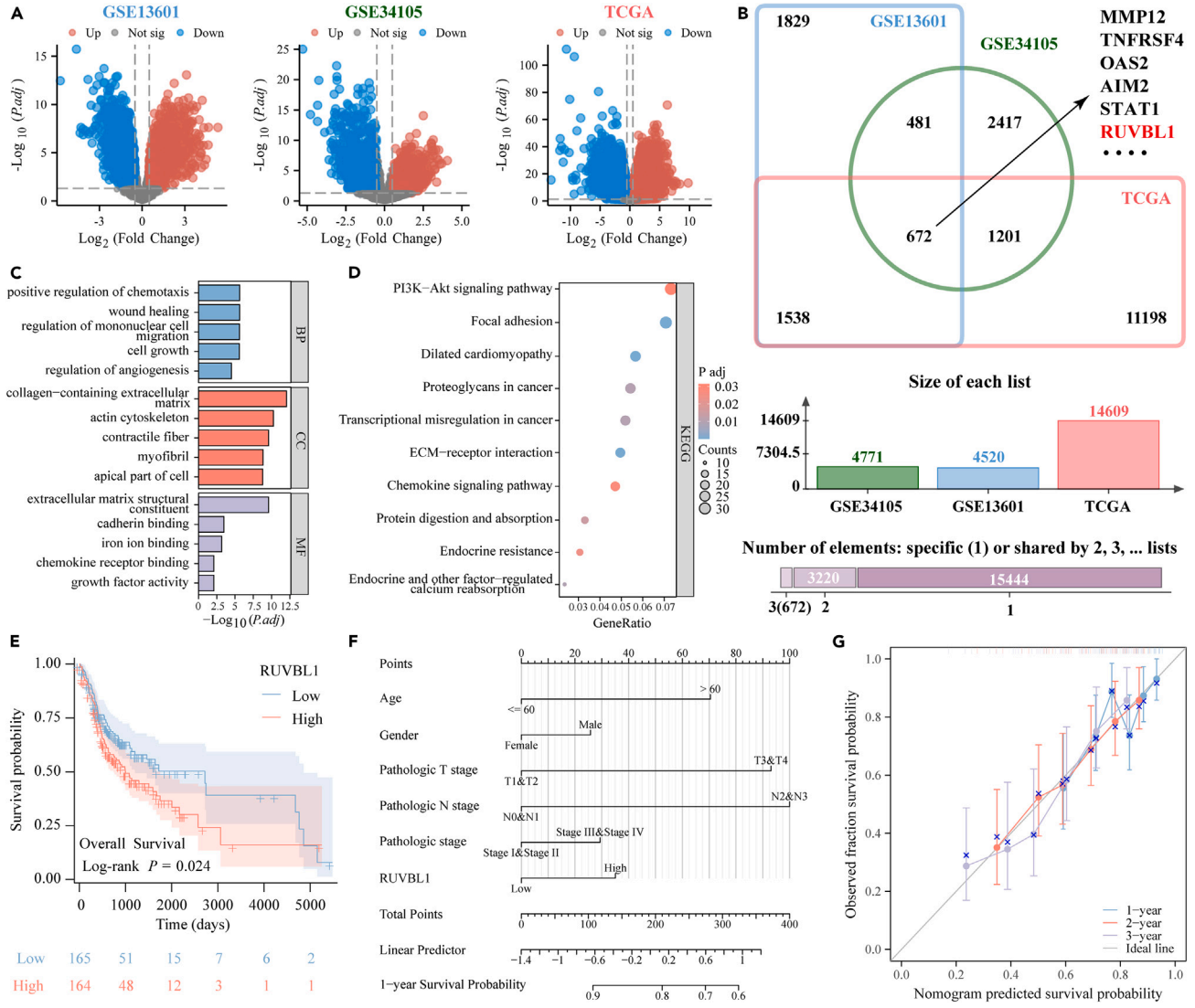

Figure 1. RUVBL1 is associated with prognosis in TSCC patients

(A) Volcano plots exhibit the number of DE-mRNAs in the TSCC-related datasets GSE13601, GSE34105, and TCGA.

(B) Venn diagram displays the number of intersecting DE-mRNAs in the GSE13601, GSE34105, and TCGA datasets.

(C and D) Bar graph (C) and bubble graph (D) show the partial GO and KEGG terms enriched by intersecting DE-mRNA, respectively.

(E) Kaplan-Meier survival curves based on log rank test demonstrates the difference in overall survival between patients with high and low expression of RUVBL1.

(F) A nomograph for predicting overall survival of TSCC patients, including age, gender, T stage, N stage, pathologic stage, and RUVBL1 expression.

(G) Calibration curves for the performance of RUVBL1-related nomographs to predict overall survival in TSCC patients at years 1, 2, and 3.

RESULTS

Identification of prognosis-associated DE-mRNA in TSCC

In this study, several TSCC-related array and high-throughput sequencing datasets (TCGA, GSE13601, and GSE34105) were characterized for differentially expressed mRNAs (DE-mRNAs) to ensure the accuracy of the screening results. Differential expression analysis based on the limma package revealed that the GSE13601 and GSE34105 datasets had 4,520 and 4,771 DE-mRNAs, which contained 2,971 upregulated and 1,549 downregulated, and 2,568 upregulated and 2,203 downregulated DE-mRNAs, respectively (Figure 1A). DESeq package-based results indicated that the TCGA-OSCC cohort had 7,798 significantly upregulated and 6,811 significantly downregulated DE-mRNAs, for a total of 14,609 DE-mRNAs (Figure 1A). Notably, the three datasets had 672 shared DE-mRNAs (Figure 1B). They mainly belonged to the extracellular matrix and were involved in biological processes such as immunity, metastasis, growth, and angiogenesis, and pathways such as PI3K-AKT, chemokine, and transcription misregulation in cancer (Figures 1C and 1D; Data S1).

Table 1. Cox regression analysis of clinical information and RUVBL1 expression in the TCGA-OSCC cohort

		Univariate analysis		Multivariate analysis	
Characteristics	Total (N)	Hazard ratio (95% CI)	p value	Hazard ratio (95% CI)	p value
Age	329				
≤ 60	156	1.330 (0.961–1.840)	0.085	1.570 (1.075–2.293)	**0.020**
>60	173				
Gender	329				
Female	102	0.903 (0.645–1.266)	0.555		
Male	227				
T stage	304				
T1&T2	128	2.420 (1.657–3.534)	**< 0.001**	1.905 (1.081–3.355)	**0.026**
T3&T4	176				
N stage	275				
N0&N1	167	2.430 (1.690–3.495)	**< 0.001**	2.022 (1.359–3.009)	**< 0.001**
N2&N3	108				
Pathologic stage	298				
Stage I & Stage II	70	2.161 (1.368–3.414)	**< 0.001**	1.274 (0.559–2.901)	0.564
Stage III & Stage IV	228				
RUVBL1	329				
Low	165	1.449 (1.047–2.006)	**0.025**	1.306 (0.896–1.903)	0.165
High	164				

DE-mRNAs in the GSE13601, GSE34105, and TCGA-oral squamous cell carcinoma (TCGA-OSCC) datasets are shown in Data S2. Considering the existing research advances in TSCC as well as the function and signaling pathway of DE-mRNA, we chose RUVBL1, a CRAF-binding protein we previously identified,[15] for subsequent prognostic analysis. Log rank test based on the TCGA dataset displayed that TSCC patients with high expression of RUVBL1 had a lower overall survival than those with low expression of RUVBL1, and both were statistically significant (Figure 1E, p = 0.024). Notably, univariate Cox analysis also exhibited that high expression of RUVBL1 predicted poorer prognosis for TSCC patients, and that clinical features such as T stage, N stage, and pathologic stage were also correlates of prognosis in TSCC (Table 1). Therefore, the present study further constructed a predictive nomograph with RUVBL1 and these clinical features to quantify the predictive outcome of survival in TSCC patients. As illustrated in Figure 1F, the nomograph exhibits a greater weighting of RUVBL1 expression compared to gender and pathologic stage. Calibration curves revealed that the predictive performance of the nomograph model was generally consistent with actual observations in the first and second years, and poorer in the third year (Figure 1G). The aforementioned results suggest that RUVBL1 has a good prognostic value in TSCC patients, and it may be one of the factors driving the TSCC process.

RUVBL1 contributes to TSCC proliferation and stemness *in vitro*

To confirm the hypothesis of this study, we explored the effect of differential expression of RUVBL1 on malignant biological behavior in TSCC cells (CAL-27 and SCC-4 cells). First, this study screened lentiviruses for RUVBL1 overexpression and knockdown. Infection with RUVBL1-overexpressing lentivirus resulted in upregulation of RUVBL1 protein and mRNA expression in CAL-27 and SCC-4 cells (Figures 2A, 2C, S1A, and S1C). Infection with short hairpin RNA (shRNA) lentivirus significantly reduced not only the mRNA expression but also the protein level of RUVBL1 in CAL-27 and SCC-4 cells (Figures 2B, 2D, S1B, and S1D). Lentiviral knockdown of sh-RUVBL1-1 and sh-RUVBL1-2 was the most effective, and they were the choices for subsequent experiments. In this study, Cell Counting Kit-8 (CCK-8) assay was applied to characterize the changes in cell activity (optical density [OD] 450 nm) of CAL-27 and SCC-4 cells that exogenously regulate RUVBL1 at 12, 24, 48, and 72 h. Compared to controls, overexpression of RUVBL1 increased the cellular OD (450 nm) of CAL-27 and SCC-4 at 48 and 72 h, and knockdown of RUVBL1 did the opposite (Figures 2E and S1E). Colony-forming unit assay also confirmed that RUVBL1 increased number of colonies in CAL-27 and SCC-4 cells at 14 days (Figures 2F and S1F). This suggests that overexpression of RUVBL1 accelerated TSCC cell proliferation *in vitro*. Notably, overexpression of RUVBL1 significantly enhanced the area and number of spheres formation at 12 days, and the opposite result was obtained by knocking down RUVBL1 (Figures 2G and S1G). Moreover, overexpression of RUVBL1 increased the ratio of $CD44^{+}CD133^{+}$ cells in CAL-27 and SCC-4 cells, and knockdown of RUVBL1 obtained the opposite result (Figures 2H and S1H). This suggests that RUVBL1 promotes proliferation and stemness of TSCC cells *in vitro*.

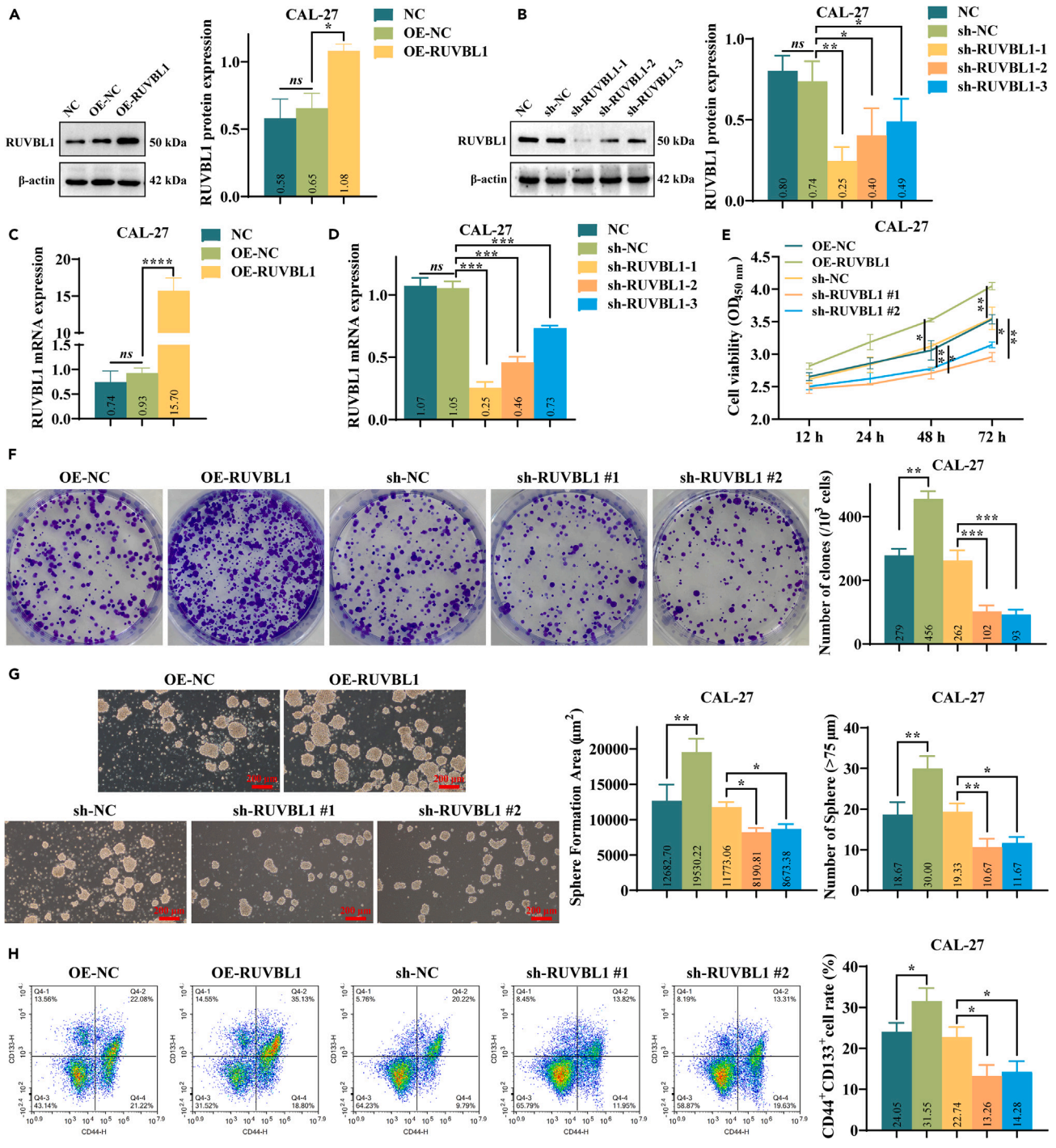

Figure 2. RUVBL1 promotes proliferation and stemness of CAL-27 cells

(A and B) Western blotting assay was performed to detect the expression of RUVBL1 protein in CAL-27 cells after infection of overexpressing (A) and knocking down (B) lentivirus.

(C and D) Following infection of RUVBL1 overexpressing (C) and knocking down (D) lentivirus, qRT-PCR assay identified changes in RUVBL1 mRNA expression in CAL-27 cells.

(E and F) CCK-8 (E) and colony-forming unit assay (F) to evaluate the proliferation and clone formation ability of CAL-27 cells after exogenous modulation of RUVBL1 expression.

(G) Sphere formation assay to reveal the effect of RUVBL1 expression on the area and number of sphere formation in CAL-27 cells. Measurement for the area and number of sphere formation was done by ImageJ software. Scale bar: 200 μm.

(H) Flow cytometry was performed to detect the proportion of CD44 and CD133 double-positive cells in each group of CAL-27 cells to reveal the effect of RUVBL1 on the stemness of CAL-27 cells. Data are represented as mean ± SD. *, **, *** and **** indicate $p < 0.05$, $p < 0.01$, $p < 0.001$ and $p < 0.0001$, respectively.

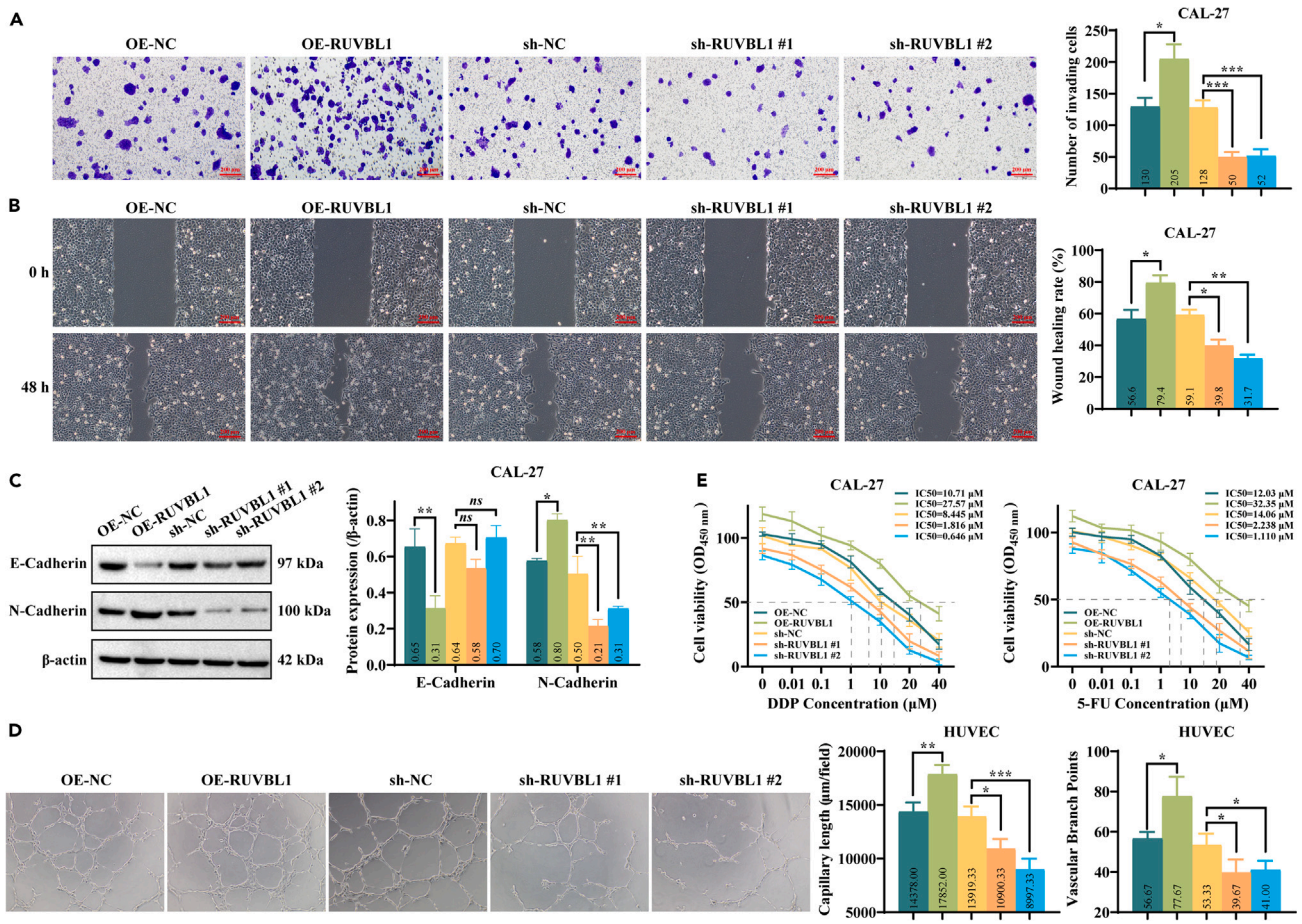

Figure 3. RUVBL1 enhances invasion, wound healing, angiogenesis, and drug resistance in CAL-27 cells

(A and B) Transwell (A) and wound healing assays (B) were performed to evaluate the number of invading cells and the percentage of wound healing in CAL-27 cells at 48 h after infection with overexpressed or knockdown RUVBL1 lentivirus, respectively. Scale bar: 200 μm.

(C) Representative images of gel blot for E-cadherin and N-cadherin in each group of CAL-27 cells.

(D) Angiogenesis experiments were performed to evaluate the effect of RUVBL1 expression on HUVEC angiogenesis, and the total length and branch points of the vessels were analyzed using ImageJ software.

(E) Changes in DDP and 5-FU sensitivity of CAL-27 cells infected with different viruses were detected by CCK-8 after treatment with different concentrations (0, 0.01, 0.1, 1, 10, 20, 40 μM) of cisplatin (DDP) and 5-fluorouracil (5-FU). Data are represented as mean ± SD. *, **, and *** indicate $p < 0.05$, $p < 0.01$, and $p < 0.001$, respectively. ns represents no significant difference.

RUVBL1 facilitates TSCC metastasis and angiogenesis *in vitro*

Previous enrichment analysis demonstrated that RUVBL1 is involved not only in cell growth but also in migration and angiogenesis (Data S1). Therefore, the present study further investigated the effects of RUVBL1 on TSCC cell metastasis and angiogenesis. Compared to controls, overexpressing RUVBL1 increased the number of invasions and the percentage of wound healing in CAL-27 and SCC-4 cells at 48 h, and knocking down RUVBL1 suppressed these phenotypes (Figures 3A, 3B, S2A, and S2B). Epithelial-mesenchymal transition (EMT) is necessary for tumor cells to leave the primary site and undergo metastasis.[16,17] Therefore, this study further examined function of RUVBL1 on the expression of EMT-related proteins in CAL-27 and SCC-4 cells. As displayed in Figures 3C and S2C, infection with overexpressed RUVBL1 lentivirus resulted in downregulation of E-cadherin and upregulation of N-cadherin in CAL-27 and SCC-4 cells, which suggests that RUVBL1 promotes EMT in TSCC cells. Notably, knockdown of RUVBL1 had no significant effect on E-cadherin but reduced N-cadherin expression in CAL-27 and SCC-4 cells (Figures 3C and S2C). Neovascularization provides access and material security for tumor cell metastasis.[18,19] Overexpression of RUVBL1 increased the length and branch points of blood vessels formed by human umbilical vein endothelial cell (HUVEC) at 6 h, and the opposite result was obtained for HUVEC infected with lentivirus knocking down RUVBL1 (Figure 3D). Moreover, the development of EMT/metastasis leads to alterations in the anti-apoptotic and metabolic profile of tumor cells, which can lead to a reduction in the killing effect of chemotherapeutic agents.[20,21] Therefore, we investigated the functions of RUVBL1 on DDP and 5-FU sensitivity in TSCC cells. As expected, overexpression of RUVBL1 increased the half-maximal inhibitory concentration (IC50) of SCC-4 and CAL-27 cells against DDP and 5-FU, and

knockdown of RUVBL1 showed inverse effect (Figures 3E and S2D). The aforementioned results suggest that RUVBL1 contributes to TSCC cell metastasis, angiogenesis, and DDP and 5-FU resistance *in vitro*.

RUVBL1 promotes TSCC progression and activates CRaf/MEK/ERK signaling *in vivo*

Further, this study explored the role of RUVBL1 in a TSCC-associated subcutaneous tumor model to fully characterize the oncogenic effects of RUVBL1. Images of nude mice and neoplasms in each group are displayed in Figure 4A. Subcutaneous injection of CAL-27 cells exogenously modulating RUVBL1 did not affect the body weight of nude mice in all groups (Figure 4B). Furthermore, overexpression of RUVBL1 enhanced the mass at 30 days and volume at 24, 27 and 30 days of neoplasms formed by CAL-27 cells, and knockdown of RUVBL1 obtained the opposite results (Figures 4C and 4D). It suggests that RUVBL1 accelerates TSCC neoplasms formation *in vivo*. Pathological staining revealed that neoplasm tissues overexpressing RUVBL1 exhibited larger nuclei, more nuclear divisions, and angiogenesis compared to controls, and neoplasm tissues knocking down RUVBL1 exhibited cell necrosis and apoptosis (Figure 4E). As expected, overexpression of RUVBL1 upregulated Ki-67 positivity in tumor tissues, and knockdown of RUVBL1 did the opposite (Figure 4F). In addition, overexpression of RUVBL1 led to increasing fluorescence intensity of the angiogenesis marker CD31 and the tumor stemness marker CD44 in neoplasm tissues, and knockdown of RUVBL1 obtained the opposite result (Figure S3). This suggests that RUVBL1 accelerates the malignant process of TSCC *in vivo*.

Notably, previous studies confirmed that RUVBL1 is a CRAF-binding protein, which leads to activation of MEK/ERK signaling.[15] We examined the effect of RUVBL1 on RAF/MEK/ERK signaling in neoplasm tissues. As expected, the expression of RUVBL1 was significantly increased in OE-RUVBL1 group, and decreased in neoplasm tissues of sh-RUVBL1#1 and sh-RUVBL1#1 groups (Figure 5A). Exogenous regulation of RUVBL1 expression had little or no significant effect on Tyr301 site phosphorylation and total protein of ARAF and Ser445 site phosphorylation and total protein of BRAF in TSCC tissues (Figures 5B and 5C). Interestingly, overexpression of RUVBL1 inhibited phosphorylation of the CRAF Ser259 (Figure 5D), an inhibitory phosphorylation site for CRAF activation.[14] This suggests that RUVBL1 inhibits Ser259 phosphorylation to contribute to CRAF activation. Further, we examined the effect of RUVBL1 on MEK/ERK signaling downstream of CRAF. As expected, overexpression of RUVBL1 significantly enhanced the phosphorylation of MEK1 and ERK1/2 in TSCC tissues, and knockdown of RUVBL1 resulted in the opposite (Figures 5E and 5F). This suggests that RUVBL1 activates MEK/ERK signaling in TSCC by inhibiting CRAF Ser259 phosphorylation.

CRAF/MEK/ERK signaling is a downstream target of RUVBL1 for cancer-promoting effects

Activation of CRAF/MEK/ERK signaling mediates tumor cell growth and metastasis.[14,22,23] Therefore, the present study set up rescue experiments using GW5074 (a specific CRAF Ser259 phosphorylation inhibitor) and PD98059 (MEK phosphorylation inhibitor) to explore the role of CRAF/MEK/ERK signaling in the oncogenic effects of RUVBL1. Treatment with PD98059 reverted the increased phosphorylation of MEK1 and ERK caused by overexpression of RUVBL1 (Figure 6A). Functional experiments demonstrated that PD98059 resulted in recovery of the increase in cellular OD (450 nm) at 48 and 72 h, and number of colonies at 14 days caused by overexpression of RUVBL1 (Figures 6B and 6C). Compared to the OE-RUVBL1 group, PD98059 significantly decreased the number and area of sphere formation at 14 days, the number of invading cells at 48 h, the percentage of wound healing at 48 h, N-cadherin expression, and DDP and 5-FU resistance in CAL-27 cells (Figures 6D–6H). Notably, GW5074 limited the decrease in malignant phenotype of CAL-27 cells induced by knockdown of RUVNL1 (Figure S4). The aforementioned results suggest that the promoting effect of RUVBL1 on the malignant biological behaviors of TSCC cells is achieved by activating CRAF/MEK/ERK signaling.

DISCUSSION

RUVBL1 is one of the major members of the AAA ATPase superfamily and often acts in concert with RUVBL2 to form multimers.[24,25] RUVBL1 is distributed in the nucleus, cytoplasm, cell membrane, and many organelles, and its main molecular function is to regulate ATPase activity and binding to cadherin, which is involved in the regulation of nuclear division, chromosome structure, DNA repair and recombination, metabolism, and cell growth and metastasis.[24] In this study, we found that RUVBL1 was identified as DE-mRNA in both the GSE13601 and GSE34105 microarrays, and the TCGA-OSCC RNA sequencing (RNA-seq) dataset. Furthermore, the expression level of RUVBL1 was related with the prognosis of TSCC patients, and RUVBL1-related nomographs have superior predictive performance for the survival of TSCC patients. This result is similar to the findings of Fang et al.,[26] who identified RUVBL1 as one of the OSCC-associated hub genes using weighted correlation network analysis, and its high expression predicted a poorer prognosis for patients. This predicts that RUVBL1 may be involved in the developmental process of TSCC. Due to its properties in cell growth and metastasis, RUVBL1 has now been proven to participate in progression of head and neck squamous cancers,[27] oral squamous cell carcinoma,[28] osteosarcoma,[29] colorectal cancer,[30] hepatocellular carcinoma,[31] breast cancer,[32] and lung cancer[33] by mediating multiple signaling pathways. Chen et al.[29] demonstrated that RUVBL1 accelerated histone H4K16 acetylation leading to chromatin remodeling, which promotes activation of the β-catenin/LEF1 complex and osteosarcoma progression. Furthermore, RUVBL1 was shown to bind mutant TP53, which resulted in enhanced transcriptional activity of mutant TP53 to promote anchorage-independent growth and metastasis of hepatocellular carcinoma.[31] Similar to these findings, the present study also confirmed that RUVBL1 contributes as an oncogenic factor to TSCC growth, metastasis, stemness, angiogenesis, and DDP and 5-FU resistance. This finding enriches the function of RUVBL1 in pan-cancer process. In contrast to the aforementioned studies, the present study also demonstrated that CRAF/MEK/ERK is a downstream pathway in which RUVBL1 functions.

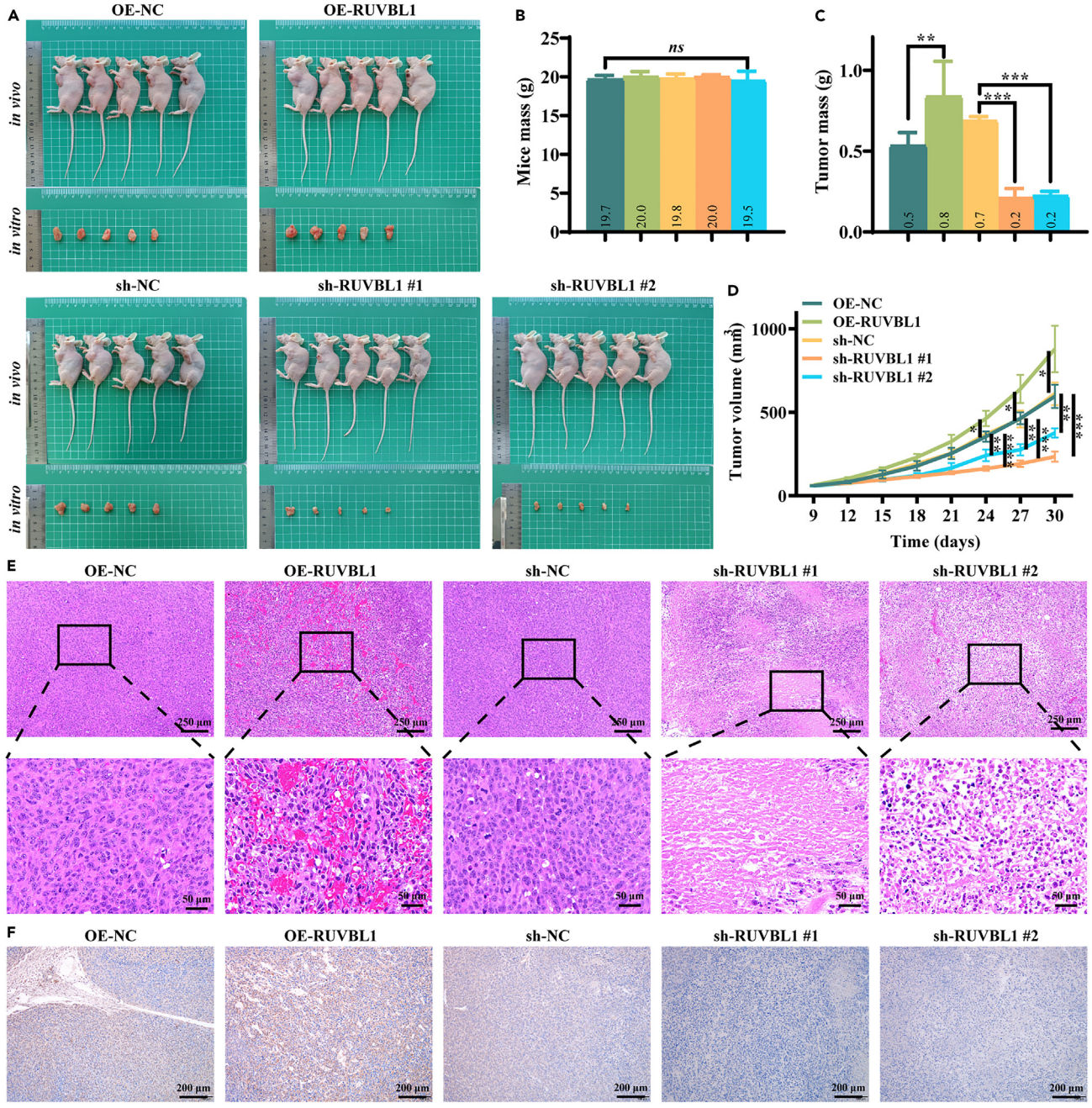

Figure 4. RUVBL1 accelerates TSCC tumor growth *in vivo*

(A) Representative images of CAL-27 cell-associated tumors *in vitro* and *ex vivo* at 30 days.

(B and C) mass of nude mice (B) and mass of CAL-27 cell-associated tumors (C) at day 30 in each group of TSCC-associated subcutaneous tumor models.

(D) Changes in volume of CAL-27 cell-associated tumors in TSCC-associated subcutaneous tumor models in each group at days 9–30.

(E) Representative H&E images of CAL-27 cell-associated tumor tissues in each group. Scale bar: 250 or 50 μm.

(F) IHC staining identified changes of Ki-67 positivity in tumor tissues from each group. Scale bar: 200 μm. Data are represented as mean ± SD. *, **, ***, and **** indicate $p < 0.05$, $p < 0.01$, $p < 0.001$, and $p < 0.0001$, respectively. ns represents no significant difference.

The oncogenic role of RAF/MEK/ERK pathway activity in malignant tumors is well established. In the present study, we found that RUVBL1 inhibits the phosphorylation of CRAF Ser259 but has no effect on the phosphorylation of ARAF Tyr301 and BRAF Ser445. Notably, Ser259 is an inhibitory site for CRAF phosphorylation, and its inhibition leads to activation of CRAF to initiate the downstream MEK/ERK pathway.[14,34] This phenomenon was also confirmed in the cell and animal experiments of this study. Furthermore, previous studies have demonstrated that

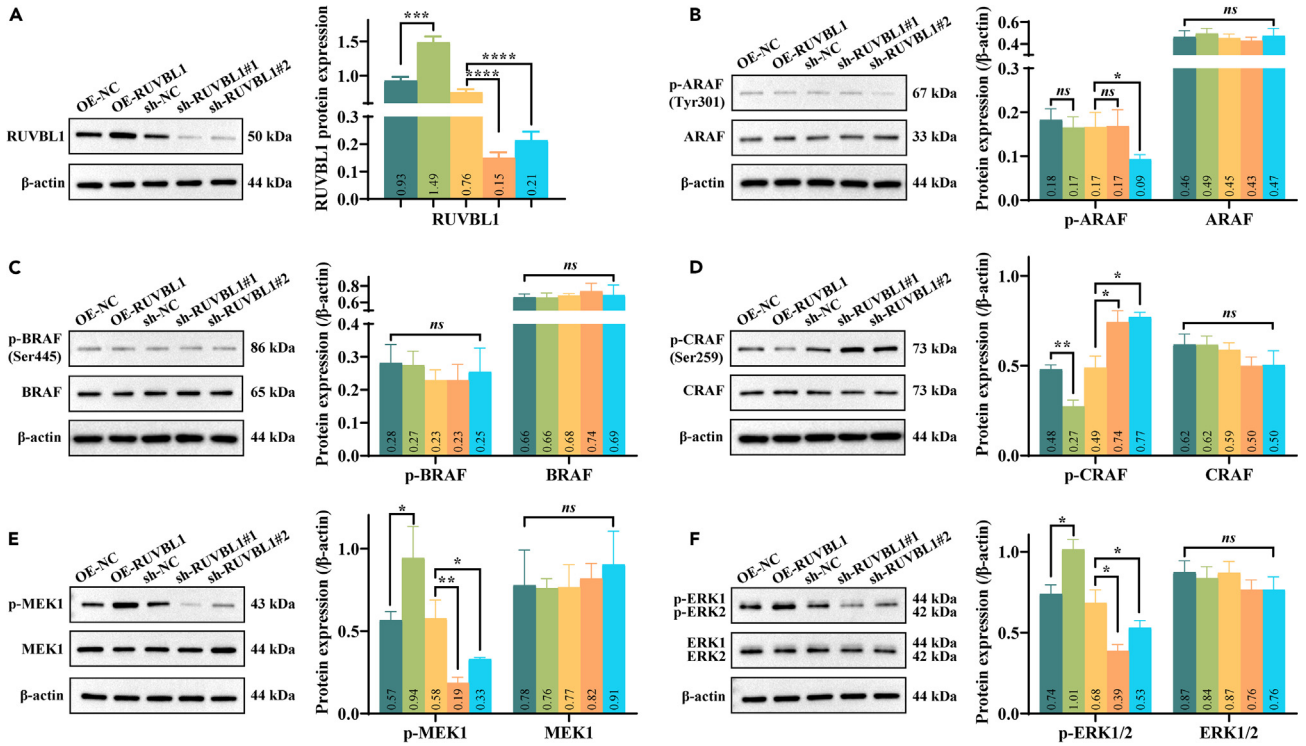

Figure 5. RUVBL1 activates CRAF/MEK/ERK signaling in TSCC tumor tissues

(A–F) Western blotting was performed to detect the expression of RUVBL1 (A), *p*-ARAF (Tyr301)/ARAF (B), *p*-BRAF (Ser445)/BRAF (C), *p*-CRAF (Ser259)/CRAF (D), *p*-MEK1/MEK (E), and *p*-ERK1/2/ERK1/2 (F). Data are represented as mean ± SD. *, **, ***, and **** indicate $p < 0.05$, $p < 0.01$, $p < 0.001$, and $p < 0.0001$, respectively. ns represents no significant difference.

aberrant activation of the CRAF/MEK/ERK pathway enhances growth, metastasis, stemness, and drug resistance in HNSCC,[35,36] which is consistent with the role of RUVBL1 in TSCC. To explore the role of the CRAF/MEK/ERK pathway in the cancer-promoting effects of RUVBL1, we blocked the RAF/MEK/ERK pathway *in vitro*. Interestingly, the present study found that GW5074 and PD98059 could specifically block CRAF Ser259 phosphorylation and MEK phosphorylation, respectively, which led to the restriction of the oncogenic role of RUVBL1 in TSCC. This suggests that the contribution of RUVBL1 to the malignant phenotype of TSCC is at least through activation of the CRAF/MEK/ERK pathway. Notably, Zhang et al.[37,38] demonstrated that RUVBL1 interacts with RAF in HEK293 cells by protein mass spectrometry and co-immunoprecipitation. The findings of this study expanded the value of RUVBL1 interactions with RAF in TSCC.

In conclusion, the present study shows that RUVBL1 activates the downstream MEK/ERK pathway by inhibiting CRAF Ser259 phosphorylation, which leads to the development of TSCC *in vivo* and *in vitro*. The present study uncovered the role of RUVBL1 in TSCC, which provides a solid experimental basis for RUVBL1 as a therapeutic target for TSCC in the future.

Limitations of the study

Admittedly, there are some shortcomings in this study. Although the present study confirms that RUVBL1 inhibits CRAF Ser259 phosphorylation and previous studies have demonstrated that RUVBL1 interacts with RAF in HEK293, it remains unknown whether RUVBL1 activates RAF in a manner that is only phosphorylated for modification and whether other phosphorylation sites are involved.

STAR★METHODS

Detailed methods are provided in the online version of this paper and include the following:

- KEY RESOURCES TABLE
- RESOURCE AVAILABILITY
  - Lead contact
  - Materials availability
  - Data and code availability
- EXPERIMENTAL MODEL AND STUDY PARTICIPANT DETAILS
  - Cells lines

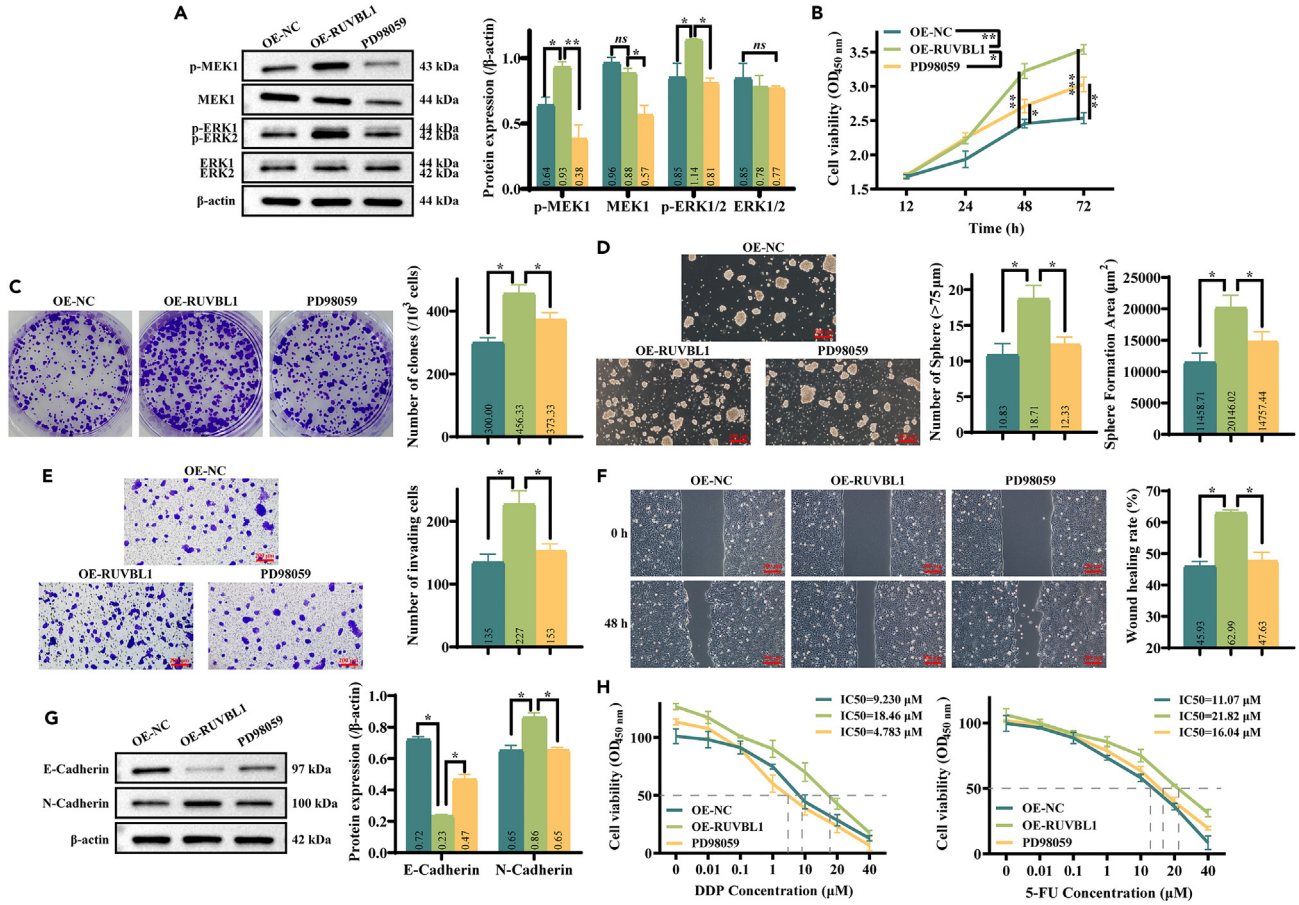

Figure 6. PD98059 restricts malignant phenotype promotion in CAL-27 cells induced by RUVBL1 overexpression

(A) Western blotting was performed to investigate the effect of PD98059 on MEK/ERK signaling in CAL-27 cells.

(B and C) CCK-8 and clone formation assays were performed to detect the effects of PD98059 on CAL-27 cell viability (B) and clone formation ability (C), respectively.

(D–F) Representative pictures of sphere formation (D), invasion (E), and wound healing (F) of CAL-27 cells in each group. Scale bar: 200 μm.

(G) Representative images of gel blot of EMT-related proteins E-cadherin and N-cadherin and statistical analysis of their expression.

(H) CCK-8 assay was performed to evaluate the viability of CAL-27 cells at different concentrations of cisplatin (DDP) and 5-fluorouracil (5-FU). Data are represented as mean ± SD. *, **, and *** indicate $p < 0.05$, $p < 0.01$, and $p < 0.001$, respectively. ns represents no significant difference.

SUPPLEMENTAL INFORMATION

Supplemental information can be found online at https://doi.org/10.1016/j.isci.2024.109434.

ACKNOWLEDGMENTS

We thank the TCGA and GEO databases and the corresponding contributors for uploading their meaningful datasets. The following funds are gratefully acknowledged for their support of this research: National Natural Science Foundation of China (grant no. 81860481, 82103049), High-End Talent Grant of Yunnan Province, China (grant no. KH-SWR-QNBJ-2020-002), Basic Research Special Youth Project of Yunnan Provincial Department of Science and Technology (grant no. 202201AU070015), Yunnan Provincial Department of Science and Technology Kunming Medical Joint Special General Project (grant no. 202201AY070001-233, 202201AY070001-231), and Midwest Orthodontics Research Project of the Youth Clinical Research Fund of the Chinese Stomatological Association (grant no. CSA-MWO2021-15).

AUTHOR CONTRIBUTIONS

X.-y.Z. and H.G. conceived and designed the experiments; X.-y.Z., Y.L., Q.R., and M.-y.Q. performed the experiments; X.-y.Z. and Y.L. analyzed and interpreted the data; R.L. provided resources; X.-y.Z. wrote the paper; Y.L., Q.R., M.-y.Q., and H.G. reviewed and edited the paper. All authors have read and agreed to the published version of the manuscript.

DECLARATION OF INTERESTS

The authors declare no competing interests.

Received: October 7, 2023
Revised: December 15, 2023
Accepted: March 4, 2024
Published: March 6, 2024

REFERENCES

1. Johnson, D.E., Burtness, B., Leemans, C.R., Lui, V.W.Y., Bauman, J.E., and Grandis, J.R. (2020). Head and neck squamous cell carcinoma. Nat. Rev. Dis. Prim. *6*, 92. https://doi.org/10.1038/s41572-020-00224-3.
2. Matsuo, K., Akiba, J., Kusukawa, J., and Yano, H. (2022). Squamous cell carcinoma of the tongue: subtypes and morphological features affecting prognosis. Am. J. Physiol. Cell Physiol. *323*. C1611-c1623. https://doi.org/10.1152/ajpcell.00098.2022.
3. Caponio, V.C.A., Troiano, G., Togni, L., Zhurakivska, K., Santarelli, A., Laino, L., Rubini, C., Lo Muzio, L., and Mascitti, M. (2023). Pattern and localization of perineural invasion predict poor survival in oral tongue carcinoma. Oral Dis. *29*, 411–422. https://doi.org/10.1111/odi.13900.
4. Melo, B.A.d.C., Vilar, L.G., Oliveira, N.R.d., Lima, P.O.d., Pinheiro, M.d.B., Domingueti, C.P., and Pereira, M.C. (2021). Human papillomavirus infection and oral squamous cell carcinoma - a systematic review. Braz. J. Otorhinolaryngol. *87*, 346–352. https://doi.org/10.1016/j.bjorl.2020.10.017.
5. Nokovitch, L., Maquet, C., Crampon, F., Taihi, I., Roussel, L.M., Obongo, R., Virard, F., Fervers, B., and Deneuve, S. (2023). Oral Cavity Squamous Cell Carcinoma Risk Factors: State of the Art. J. Clin. Med. *12*, 3264. https://doi.org/10.3390/jcm12093264.
6. Ng, J.H., Iyer, N.G., Tan, M.H., and Edgren, G. (2017). Changing epidemiology of oral squamous cell carcinoma of the tongue: A global study. Head Neck *39*, 297–304. https://doi.org/10.1002/hed.24589.
7. da Silva Souto, A.C., Vieira Heimlich, F., Lima de Oliveira, L., Bergmann, A., Dias, F.L., Spíndola Antunes, H., de Melo, A.C., Thuler, L.C.S., and Cohen Goldemberg, D. (2023). Epidemiology of tongue squamous cell carcinoma: A retrospective cohort study. Oral Dis. *29*, 402–410. https://doi.org/10.1111/odi.13897.
8. Kitamura, N., Sento, S., Yoshizawa, Y., Sasabe, E., Kudo, Y., and Yamamoto, T. (2020). Current Trends and Future Prospects of Molecular Targeted Therapy in Head and Neck Squamous Cell Carcinoma. Int. J. Mol. Sci. *22*, 240. https://doi.org/10.3390/ijms22010240.
9. Yamauchi, M., Minesaki, A., Ishida, T., Sato, Y., Okamura, S., Shuto, H., Tanaka, N., Hatayama, E., Shibamiya, N., and Kuratomi, Y. (2023). Induction Chemotherapy With 5-Fluorouracil, Cisplatin, and Cetuximab in Advanced Head and Neck Squamous Cell Carcinoma. In Vivo *37*, 1275–1280. https://doi.org/10.21873/invivo.13205.
10. Keil, F., Hartl, M., Altorjai, G., Berghold, A., Riedl, R., Pecherstorfer, M., Mayrbäurl, B., De Vries, A., Schuster, J., Hackl, J., et al. (2021). Docetaxel, Cisplatin and 5-FU Compared with Docetaxel, Cisplatin and Cetuximab as Induction Chemotherapy in Advanced Squamous Cell Carcinoma of the Head and Neck: Results of a Randomised Phase II AGMT Trial*151* (European journal of cancer), pp. 201–210. https://doi.org/10.1016/j.ejca.2021.03.051.
11. Ayati, A., Moghimi, S., Salarinejad, S., Safavi, M., Pouramiri, B., and Foroumadi, A. (2020). A review on progression of epidermal growth factor receptor (EGFR) inhibitors as an efficient approach in cancer targeted therapy. Bioorg. Chem. *99*, 103811. https://doi.org/10.1016/j.bioorg.2020.103811.
12. Levantini, E., Maroni, G., Del Re, M., and Tenen, D.G. (2022). EGFR signaling pathway as therapeutic target in human cancers. Semin. Cancer Biol. *85*, 253–275. https://doi.org/10.1016/j.semcancer.2022.04.002.
13. Degirmenci, U., Wang, M., and Hu, J. (2020). Targeting Aberrant RAS/RAF/MEK/ERK Signaling for Cancer Therapy. Cells *9*. https://doi.org/10.3390/cells9010198.
14. Ullah, R., Yin, Q., Snell, A.H., and Wan, L. (2022). RAF-MEK-ERK pathway in cancer evolution and treatment. Semin. Cancer Biol. *85*, 123–154. https://doi.org/10.1016/j.semcancer.2021.05.010.
15. Guo, H., Zhang, X.Y., Peng, J., Huang, Y., Yang, Y., Liu, Y., Guo, X.X., Hao, Q., An, S., and Xu, T.R. (2018). RUVBL1, a novel C-RAF-binding protein, activates the RAF/MEK/ERK pathway to promote lung cancer tumorigenesis. Biochem. Biophys. Res. Commun. *498*, 932–939. https://doi.org/10.1016/j.bbrc.2018.03.084.
16. Huang, Y., Hong, W., and Wei, X. (2022). The molecular mechanisms and therapeutic strategies of EMT in tumor progression and metastasis. J. Hematol. Oncol. *15*, 129. https://doi.org/10.1186/s13045-022-01347-8.
17. Fedele, M., Sgarra, R., Battista, S., Cerchia, L., and Manfioletti, G. (2022). The Epithelial-Mesenchymal Transition at the Crossroads between Metabolism and Tumor Progression. Int. J. Mol. Sci. *23*, 800. https://doi.org/10.3390/ijms23020800.
18. Yang, Y., and Cao, Y. (2022). The impact of VEGF on cancer metastasis and systemic disease. Semin. Cancer Biol. *86*, 251–261. https://doi.org/10.1016/j.semcancer.2022.03.011.
19. Majidpoor, J., and Mortezaee, K. (2021). Angiogenesis as a hallmark of solid tumors - clinical perspectives. Cell. Oncol. *44*, 715–737. https://doi.org/10.1007/s13402-021-00602-3.
20. Hashemi, M., Arani, H.Z., Orouei, S., Fallah, S., Ghorbani, A., Khaledabadi, M., Kakavand, A., Tavakolpournegari, A., Saebfar, H., Heidari, H., et al. (2022). EMT mechanism in breast cancer metastasis and drug resistance: Revisiting molecular interactions and biological functions. Biomedicine & pharmacotherapy = Biomedecine & pharmacotherapie *155*, 113774. https://doi.org/10.1016/j.biopha.2022.113774.
21. De Las Rivas, J., Brozovic, A., Izraely, S., Casas-Pais, A., Witz, I.P., and Figueroa, A. (2021). Cancer drug resistance induced by EMT: novel therapeutic strategies. Arch. Toxicol. *95*, 2279–2297. https://doi.org/10.1007/s00204-021-03063-7.

22. Wu, P.K., Becker, A., and Park, J.I. (2020). Growth Inhibitory Signaling of the Raf/MEK/ERK Pathway. Int. J. Mol. Sci. *21*, 5436. https://doi.org/10.3390/ijms21155436.
23. Guo, Y.J., Pan, W.W., Liu, S.B., Shen, Z.F., Xu, Y., and Hu, L.L. (2020). ERK/MAPK signalling pathway and tumorigenesis. Exp. Ther. Med. *19*, 1997–2007. https://doi.org/10.3892/etm.2020.8454.
24. Dauden, M.I., López-Perrote, A., and Llorca, O. (2021). RUVBL1-RUVBL2 AAA-ATPase: a versatile scaffold for multiple complexes and functions. Curr. Opin. Struct. Biol. *67*, 78–85. https://doi.org/10.1016/j.sbi.2020.08.010.
25. Izumi, N., Yamashita, A., Iwamatsu, A., Kurata, R., Nakamura, H., Saari, B., Hirano, H., Anderson, P., and Ohno, S. (2010). AAA+ proteins RUVBL1 and RUVBL2 coordinate PIKK activity and function in nonsense-mediated mRNA decay. Sci. Signal. *3*, ra27. https://doi.org/10.1126/scisignal.2000468.
26. Fang, Z., Wang, F., Zhang, M., Huang, H., and Lin, Z. (2022). Identification of Co-Expression Modules and Genes Associated With Tumor Progression in Oral Squamous Cell Carcinoma. Pathol. Oncol. Res. *28*, 1610481. https://doi.org/10.3389/pore.2022.1610481.
27. Lin, D., Lin, B., Bhanot, H., Riou, R., Abt, N.B., Rajagopal, J., and Saladi, S.V. (2020). RUVBL1 is an amplified epigenetic factor promoting proliferation and inhibiting differentiation program in head and neck squamous cancers. Oral Oncol. *111*, 104930. https://doi.org/10.1016/j.oraloncology.2020.104930.
28. Zeng, Y., Kong, Y., Liao, L., and Zhu, H. (2022). Involvement of RUVBL1 in WNT/β-Catenin Signaling in Oral Squamous Cell Carcinoma. Dis. Markers *2022*, 3398492. https://doi.org/10.1155/2022/3398492.
29. Chen, J., Liu, G., Wu, Y., Ma, J., Wu, H., Xie, Z., Chen, S., Yang, Y., Wang, S., Shen, P., et al. (2019). CircMYO10 promotes osteosarcoma progression by regulating miR-370-3p/RUVBL1 axis to enhance the transcriptional activity of β-catenin/LEF1 complex via effects on chromatin remodeling. Mol. Cancer *18*, 150. https://doi.org/10.1186/s12943-019-1076-1.
30. Liu, X., Chen, J., Zhang, S., Liu, X., Long, X., Lan, J., Zhou, M., Zheng, L., and Zhou, J. (2022). LINC00839 promotes colorectal cancer progression by recruiting RUVBL1/Tip60 complexes to activate NRF1. EMBO Rep. *23*, e54128. https://doi.org/10.15252/embr.202154128.
31. Zhao, Y., Zhang, C., Yue, X., Li, X., Liu, J., Yu, H., Belyi, V.A., Yang, Q., Feng, Z., and Hu, W. (2015). Pontin, a new mutant p53-binding protein, promotes gain-of-function of mutant p53. Cell Death Differ. *22*, 1824–1836. https://doi.org/10.1038/cdd.2015.33.
32. Fan, W., Xie, J., Xia, J., Zhang, Y., Yang, M., Wang, H., Pan, Y., Zhang, M., Han, B., Wu, B., et al. (2017). RUVBL1-ITFG1 interaction is required for collective invasion in breast cancer. Biochim. Biophys. Acta Gen. Subj. *1861*, 1788–1800. https://doi.org/10.1016/j.bbagen.2017.03.016.
33. Yenerall, P., Das, A.K., Wang, S., Kollipara, R.K., Li, L.S., Villalobos, P., Flaming, J., Lin, Y.F., Huffman, K., Timmons, B.C., et al. (2020). RUVBL1/RUVBL2 ATPase Activity Drives PAQosome Maturation, DNA Replication and Radioresistance in Lung Cancer. Cell Chem. Biol. *27*, 105–121.e14. https://doi.org/10.1016/j.chembiol.2019.12.005.
34. Liu, F., Yang, X., Geng, M., and Huang, M. (2018). Targeting ERK, an Achilles' Heel of the MAPK pathway, in cancer therapy. Acta Pharm. Sin. B *8*, 552–562. https://doi.org/10.1016/j.apsb.2018.01.008.
35. Kashyap, T., Pramanik, K.K., Nath, N., Mishra, P., Singh, A.K., Nagini, S., Rana, A., and Mishra, R. (2018). Crosstalk between Raf-MEK-ERK and PI3K-Akt-GSK3β signaling networks promotes chemoresistance, invasion/migration and stemness via expression of CD44 variants (v4 and v6) in oral cancer. Oral Oncol. *86*, 234–243. https://doi.org/10.1016/j.oraloncology.2018.09.028.
36. Dey, S., Singh, A.K., Singh, A.K., Rawat, K., Banerjee, J., Agnihotri, V., and Upadhaya, D. (2022). Critical pathways of oral squamous cell carcinoma: molecular biomarker and therapeutic intervention. Med. Oncol. *39*, 30. https://doi.org/10.1007/s12032-021-01633-4.
37. Zhang, X.Y., Guo, H., Huang, Y., Hao, P.Q., Yang, Y., Liu, Y., Guo, X.X., Hao, Q., An, S., and Xu, T.R. (2019). Comparative interactome analysis reveals distinct and overlapping properties of Raf family kinases. Biochem. Biophys. Res. Commun. *514*, 1217–1223. https://doi.org/10.1016/j.bbrc.2019.05.089.
38. Zhang, X.Y., Guo, H., Han, B., Zhang, X.M., Huang, Y., Yang, Y., Liu, Y., Guo, X.X., Hao, Q., An, S., and Xu, T.R. (2018). Revealing A-Raf functions through its interactome. Biochim. Biophys. Acta, Proteins Proteomics *1866*, 849–856. https://doi.org/10.1016/j.bbapap.2018.05.009.
39. Estilo, C.L., O-charoenrat, P., Talbot, S., Socci, N.D., Carlson, D.L., Ghossein, R., Williams, T., Yonekawa, Y., Ramanathan, Y., Boyle, J.O., et al. (2009). Oral tongue cancer gene expression profiling: Identification of novel potential prognosticators by oligonucleotide microarray analysis. BMC Cancer *9*, 11. https://doi.org/10.1186/1471-2407-9-11.
40. Rentoft, M., Coates, P.J., Laurell, G., and Nylander, K. (2012). Transcriptional profiling of formalin fixed paraffin embedded tissue: pitfalls and recommendations for identifying biologically relevant changes. PLoS One *7*, e35276. https://doi.org/10.1371/journal.pone.0035276.
41. Liu, J., Lichtenberg, T., Hoadley, K.A., Poisson, L.M., Lazar, A.J., Cherniack, A.D., Kovatich, A.J., Benz, C.C., Levine, D.A., Lee, A.V., et al. (2018). An Integrated TCGA Pan-Cancer Clinical Data Resource to Drive High-Quality Survival Outcome Analytics. Cell *173*, 400–416.e11. https://doi.org/10.1016/j.cell.2018.02.052.
42. Ritchie, M.E., Phipson, B., Wu, D., Hu, Y., Law, C.W., Shi, W., and Smyth, G.K. (2015). limma powers differential expression analyses for RNA-sequencing and microarray studies. Nucleic Acids Res. *43*, e47. https://doi.org/10.1093/nar/gkv007.
43. Love, M.I., Huber, W., and Anders, S. (2014). Moderated estimation of fold change and dispersion for RNA-seq data with DESeq2. Genome Biol. *15*, 550. https://doi.org/10.1186/s13059-014-0550-8.
44. Wu, T., Hu, E., Xu, S., Chen, M., Guo, P., Dai, Z., Feng, T., Zhou, L., Tang, W., Zhan, L., et al. (2021). clusterProfiler 4.0: A universal enrichment tool for interpreting omics data. Innovation *2*, 100141. https://doi.org/10.1016/j.xinn.2021.100141.
45. Eng, K.H., Schiller, E., and Morrell, K. (2015). On representing the prognostic value of continuous gene expression biomarkers with the restricted mean survival curve. Oncotarget *6*, 36308–36318. https://doi.org/10.18632/oncotarget.6121.
46. Ginestet, C. (2011). ggplot2: Elegant Graphics for Data Analysis. J. Roy. Stat. Soc. Stat. Soc. *174*, 245–246. https://doi.org/10.1111/j.1467-985X.2010.00676_9.x.
47. Lin, H., and Zelterman, D. (2002). Modeling Survival Data: Extending the Cox Model. Technometrics *44*, 85–86.
48. Clough, E., and Barrett, T. (2016). The Gene Expression Omnibus Database. Methods Mol. Biol. *1418*, 93–110. https://doi.org/10.1007/978-1-4939-3578-9_5.
49. Bardou, P., Mariette, J., Escudié, F., Djemiel, C., and Klopp, C. (2014). jvenn: an interactive Venn diagram viewer. BMC Bioinf. *15*, 293. https://doi.org/10.1186/1471-2105-15-293.

STAR★METHODS

KEY RESOURCES TABLE

REAGENT or RESOURCE	SOURCE	IDENTIFIER
Antibodies		
Mouse Anti-β actin mAb	ZSGB-BIO	Cat#TA-09; RRID: AB_2636897
C-RAF	Abcam	Cat#ab181115; RRID: AB_2891010
Phospho-c-Raf (Ser259)	Abcam	Cat#ab173539; RRID: AB_2813740
Phospho-c-Raf (Ser338)	Therm Fisher	Cat#PA5-104734; RRID: AB_2816207
ERK	Abcam	Cat#ab184699; RRID: AB_2802136
p-ERK	Abcam	Cat#ab201015; RRID: AB_2934088
E-Cadherin	Abcam	Cat#ab231303; RRID: AB_2923285
N-Cadherin	Abcam	Cat#ab98952; RRID: AB_10696943
FITC-CD44 Monoclonal Antibody (IM7)	Therm Fisher	Cat#11-0441-82; RRID: AB_465045
APC-CD133 (Prominin-1) Monoclonal Antibody (TMP4)	Therm Fisher	Cat#17-1338-42; RRID: AB_1603199
Goat Anti Mouse IgG-HRP	Abmart	Cat#M21001L; RRID: AB_2713950
Goat Anti Rabbit IgG-HRP	Abmart	Cat#M21002L; RRID: AB_2713951
Bacterial and virus strains		
PGMLV-CMV-MCS-3×Flag-PGK-Puro	Genomeditech	Cat#GM-LC-132797
pGMLV-SC5 RNAi	Genomeditech	Cat#GM-LC-134309
Chemicals, peptides, and recombinant proteins		
PD98059	MCE	Cat#HY-12028
GW5074	MCE	Cat#HY-10542
cisplatin	MCE	Cat#HY-17394
5-fluorouracil	MCE	Cat#HY-90006
Critical commercial assays		
Cell Counting Kit-8 kit	DOJINDO	Cat#CK04-13
DMEM medium	Thermo Fisher	Cat#12491023
DMEM/F12 medium	Thermo Fisher	Cat#11320082
Trizol Reagent	Thermo Fisher	Cat#15596018
Taq Pro Universal SYBR qPCR Master Mix	Vazyme	Cat#Q712-02
Hematoxylin and Eosin Staining Kit	Beyotime	Cat#C0105S
FastKing RT Kit (With gDNase) FastKing cDNA	Tiangen	Cat#KR116-03
Deposited data		
GSE13601	Estilo et al.[39]	https://www.ncbi.nlm.nih.gov/geo/query/acc.cgi?acc=GSE13601
GSE34105	Rentoft et al.[40]	https://www.ncbi.nlm.nih.gov/geo/query/acc.cgi?acc=GSE34105
TCGA-OSCC	Liu[41]	https://www.cancer.gov/ccg/research/genome-sequencing/tcga
Experimental models: Cell lines		
CAL-27 cells	Procell	Cat#CL-0265
HUVEC cells	Cobioer Biosciences	Cat#CBP60340
SCC-4 cells	Cobioer Biosciences	Cat#CBP60688
Experimental models: Organisms/strains		
Subcutaneous tumor model	This paper	N/A

(Continued on next page)

Continued

REAGENT or RESOURCE	SOURCE	IDENTIFIER
Oligonucleotides		
short hairpin RNA	Genomeditech	Cat#GM-LC-134309
Software and algorithms		
R software	Lucent	https://www.r-project.org/
limma package	Ritchie et al.[42]	https://bioconductor.org/packages/release/bioc/html/limma.html
DESeq package	Love et al.[43]	https://bioconductor.org/packages//2.10/bioc/html/DESeq.html
clusterProfiler package	Wu et al.[44]	https://bioconductor.org/packages/release/bioc/html/clusterProfiler.html
rms package	Eng et al.[45]	https://cran.r-project.org/web/packages/rms/index.html
ggplot2 package	Ginestet et al.[46]	https://www.rdocumentation.org/packages/ggplot2/versions/3.4.4
ImageJ software	National Institutes of Health	https://imagej.net/software/imagej/
GraphPad Prism software	GraphPad Software	https://www.graphpad.com/scientific-software/prism/www.graphpad.com/scientific-software/prism/
survival package	Lin et al.[47]	https://cran.r-project.org/web/packages/survival/index.html
Other		
MR-96A microplate reader	Mindray	https://www.mindray.com/content/xpace/en/products/laboratory-diagnostics/elisa/mr-96a.html
Novocyte advanteon flow cytometer	Agilent	Cat#2010194
BX53 light microscope	Olympus	https://lifescience.evidentscientific.com.cn/zh/microscopes/upright/bx53f2/
GENESYS™ 40/50 Vis/UV-Vis spectrophotometer	Thermo Fisher	Cat#840-297000
Luminoskan™ Ascent Chemiluminescence Analyzer	Thermo Fisher	Cat#2805621
7500 Real Time PCR System	ABI	Cat#4351104
E0972 automatic microtome	Beyotime	Cat#E0972
VM1000 digital scanner	Motic	https://www.med.motic.com/index.php/Proservice/proServiceList/menu/pro/_id/27/fid/3.html

RESOURCE AVAILABILITY

Lead contact

Further information and requests for resources and reagents should be directed to and will be fulfilled by the lead contact, Dr. Hui Guo: (guohuiggxx@163.com)

Materials availability

This study did not generate new unique reagents.

Data and code availability

- All data reported in this paper will be shared by the lead contact upon request.
- This paper does not report original code.
- Any additional information required to reanalyze the data reported in this paper is available from the lead contact upon request.

EXPERIMENTAL MODEL AND STUDY PARTICIPANT DETAILS

Cells lines

CAL-27, HUVEC, and SCC-4 cells were purchased from Wuhan Procell Life Technology CO., LTD. and Nanjing Cobioer Biosciences CO., LTD. Cultures of SCC-4 and CAL-27 cells were performed using DMEM medium (Thermo Fisher, USA). RUVBL1 short hairpin RNA (shRNA) and its

negative control were constructed by Genomeditech Biotechnology CO., LTD. RUVBL1 shRNA and its negative controls were GGGAGTGAAGTTTACTCAACT (sh-RUVBL1-1), GCCACAGAATTCGACCTTGAA (sh-RUVBL1-2), GTCCATGATGGGCCAGCTAAT (sh-RUVBL1-3) and TTCTCCGAACGTGTCACGT (sh-NC). The vectors for RUVBL1 amplified fragments and shRNA were PGMLV-CMV-MCS-3×Flag-PGK-Puro and pGMLV-SC5 RNAi, respectively. Sequencing and lentiviral package of vectors and lentiviral titration were performed by Genomeditech. After 72 h of RUVBL1 shRNA lentivirus infection of SCC-4 and CAL-27 cells cells, shRNA lentivirus screening was performed by qRT-PCR and western blotting.

SCC-4 and CAL-27 cells were randomly divided into OE-NC, OE-RUVBL1, sh-NC, sh-RUVBL1 #1, and sh-RUVBL1 #2 groups and infected with a negative control of RUVBL1 overexpressing lentivirus, RUVBL1 overexpressing lentivirus, a negative control of RUVBL1 shRNA lentivirus, sh-RUVBL1-1 lentivirus, and sh-RUVBL1-2 lentivirus. SCC-4 and CAL-27 cells were infected with lentivirus with 72 h for subsequent experiments. CAL-27 cells of OE-RUVBL1 and sh-RUVBL1 #2 groups were separately treated with 10 μM PD98059 (MEK phosphorylation inhibitor; MCE) and 1 μM GW5074 (a specific CRAF Ser259 phosphorylation inhibitor; MCE, US) for 48 h to construct the GW5074 and PD98059 groups.

Animal studies

Balb/c-nu mice (female; 18–22 g; 6–8 weeks of age) were obtained from the Experimental Animal Center of Kunming Medical University, with a total of 25. Balb/c-nu mice were randomly divided into OE-NC, OE-RUVBL1, sh-NC, sh-RUVBL1 #1, and sh-RUVBL1 #2 groups. The left side of the forelimb of Balb/c-nu mice in each group was injected with 100 μl CAL-27 cells (5.0×10^7 cells/ml) of the corresponding group. The length and width of each group of neoplasms in the body were measured with vernier calipers from day 9. After 30 days of modeling, euthanasia was performed on each group of Balb/c-nu mice, and the mass of each group of mice and the mass of the corresponding neoplasm were weighed. Neoplasms from each group at 30 days were taken to perform tumor tissue staining. The study was approved by the Ethics Committee of Affiliated Hospital of Kunming University of Science and Technology (Approval Number: 20210228) and strictly adhered to the ARRIVE guidelines.

METHOD DETAILS

Bioinformatics-based screening of differentially expressed mRNAs associated with TSCC prognosis

TSCC-related cohorts were extracted from GEO[48] and TCGA databases, and the TCGA-OSCC, GSE13601 [39] and GSE34105 [40] datasets were finally selected. Information on the TCGA-OSCC, GSE13601, and GSE34105 datasets is provided in Table S1. Bioinformatics analyses of the three datasets were performed based on R software (V. 4.2.1), including differential expression analysis, enrichment analysis and prognostic analysis. The differential expression analysis for the GSE13601 and GSE34105 datasets was performed based on the limma package,[42] while the TCGA-OSCC dataset was performed based on the DESeq package.[43] The thresholds for differentially expressed mRNAs (DE-mRNAs) satisfy both adj. $p < 0.05$ and $|log2FC|>0.5$. Common DE-mRNAs from the three datasets were obtained based on the jvenn web[49] and GO and KEGG enrichment analysis of common DE-mRNAs was performed using clusterProfiler package.[44] Prognostic analysis of clinical information and RUVBL1 in the TCGA-ESCC dataset was performed using the survival package[47] based on Cox regression analysis (univariate and multivariate) and Log rank test and. The rms package[45] was utilized to construct a nomogram model and Calibration analysis related to clinical information and RUVBL1 in the TCGA-ESCC dataset. Prognostic data for TCGA-ESCC were derived from the integration of Liu et al.[41] The visualization of all analyzed data was performed using ggplot2,[46] rms package[45] and survminer.

TSCC cell proliferation assay

Cell proliferation of SCC-4 and CAL-27 cells was evaluated using CCK-8 kit (DOJINDO, Japan) and colony-forming unit assay. For CCK-8 experiments, 96-well plates inoculated with SCC-4 and CAL-27 cells were supplemented with 10 μl of CCK-8 solution per well. After incubation, the OD values of each group of cells were detected at 450 nm on an MR-96A microplate reader (Mindray, China). For drug sensitivity assays, SCC-4 and CAL-27 cells were treated with different concentrations (0, 0.01, 0.1, 1, 10, 20, and 40 μM) of cisplatin (DDP; MCE, US) and 5-fluorouracil (5-FU; MCE), respectively, for 48 h, and then CCK-8 experiments were performed.

For colony-forming unit assay, suspensions of logarithmic growth phase SCC-4 and CAL-27 cells were prepared using DMEM medium (ThermoFisher, US) containing 20% FBS and P/S double antibody. The concentration of SCC-4 and CAL-27 cells was adjusted, and 1000 cells were inoculated per well in a 6-well plate. According to the criteria of clone formation with the number of cells in each clone greater than 50, CAL-27 and SCC-4 cell clones were stained with crystal violet for 20 min at 14 d, and images were collected.

TSCC stemness assay

Sphere forming assay and flow cytometry were used to characterize the stemness of SCC-4 and CAL-27 cells. For the Sphere forming assay, logarithmic growth phase SCC-4 and CAL-27 cells from each group were cultured in 24-well plates with 500 cells/well, which contained serum-free DMEM/F12 medium (ThermoFisher) with 20 ng/ml EGF, 2% B27, 2 mmol/L glutamine, 1% sodium pyruvate, and 10 ng/ml bFGF. Sphere images were collected at 12 d, according to the situation of sphere formation. Flow cytometry was applied to detect $CD44^+CD133^+$ cells to identify TSCC stemness. SCC-4 and CAL-27 cells of each group were digested by trypsin and centrifuged at 1000 rmp for 3 min to collect the cells. SCC-4 and CAL-27 cells of each group were divided into four equal parts for blank control, CD44 mono-staining control, CD133 mono-staining control and CD44CD133 double-staining experiments, respectively. CD44 mono-staining control, CD133 mono-staining control and CD44CD133 double-staining experiments were incubated with 5 μl FITC-CD44 Monoclonal Antibody (IM7), 5 μl APC-CD133 (Prominin-1)

Monoclonal Antibody (TMP4), and both for 30 min, respectively. Antibody information is provided in Table S2. All samples were assayed in a Novocyte advanteon flow cytometer (Agilent, US), and the results were gated with a blank control as an isotype control to determine the positive rate of $CD44^{+}CD133^{+}$ cells in each group.

TSCC cell metastasis assay

In vitro metastasis of SCC-4 and CAL-27 cells in each group was assessed by Transwell assay for invasion and wound healing assay for migration. For Transwellassay, 50 μl of serum-free medium-diluted matrigel (1:8; Corning, USA) was spread on the bottom of the upper chamber of the Transwell (Corning, USA). The lower chamber of the Transwell was supplemented with 200 μl of SCC-4 and CAL-27 cell suspension, approximately 2×10^4 cells, and 500 μl of DMEM medium was added to the lower chamber of the Transwell. SCC-4 and CAL-27 cells in the lower chamber of Transwell were stained with crystal violet (MCE, USA) for 5 min after 48 h of culture. For the wound healing assay, 100 μl of SCC-4 and CAL-27 cells ($2.5X10^4$ cells/ml) were sequentially inoculated into two wells of the Ibidi insert (Ibidi, Germany). The following day, Ibidi inserts were removed. After 48 h of incubation, representative pictures of the wound healing assay were collected. A BX53 light microscope (Olympus, Japan) was used to collect representative images of Transwell and wound healing assays

Angiogenesis assay

HUVEC cells were randomly divided into OE-NC, OE-RUVBL1, sh-NC, sh-RUVBL1 #1, and sh-RUVBL1 #2 groups and subjected to infection with the corresponding lentiviruses. The 200 μl of HUVEC cells at a concentration of 2×10^5 cells/ml were inoculated on Matrigel (Corning, US) mixed with DMEM medium. After 5–6 h of incubation, a BX53 light microscope (Olympus, Japan) was performed for observation and image collection of HUVEC cell angiogenesis. Blood vessel length and branch points were determined using the Angiogenesis Analyzer plug-in for Image J software (NIH, US).

Western blotting assay

Total proteins from each group of SCC-4 and CAL-27 cells and neoplasms were extracted using RIPA lysate and the concentrations were determined by GENESYS™ 40/50 Vis/UV-Vis spectrophotometer (ThermoFisher). After equal amounts of total proteins were subjected to SDS-PAGE electrophoresis, they were transferred to PVDF membranes and closed with 5% skimmed milk powder. After incubation of PVDF membranes with primary and secondary antibodies against the target proteins. Exposure and image collection of PVDF membranes were performed by Luminoskan™ Ascent Chemiluminescence Analyzer (ThermoFisher). Antibody information for the target protein is provided in Table S2.

qRT-PCR assay

RUVBL1 mRNA was detected. Total RNA extraction, total RNA reverse transcription, and amplification of RUVBL1 mRNA in each group of SCC-4 and CAL-27 cells and neoplasms were performed using Trizol Reagent (ThermoFisher), FastKing RT Kit (With gDNase) FastKing cDNA (Tiangen, Germany) and Taq Pro Universal SYBR qPCR Master Mix (Vazyme, China). The primer sequences were GCAGGAGTACGATGAGTCCG (β-actin-F), ACGCAGCTCAGTAACAGTCC (β-actin-R), CACTGAGGACATCACATC (RUVBL1-F) and CTGAGTACCTGTTTCATTTC (RUVBL1-R). The 7500 Real Time PCR System (ABI, US) performed the measurement of Ct for RUVBL1 mRNA.

Tumor tissue staining

The neoplasm in each group were fixed, dehydrated, permeabilized, and embedded using 4% neutral paraformaldehyde, ethanol, xylene, and paraffin, respectively. Subsequently, neoplasm tissue sections with 5 μm were prepared using the E0972 automatic microtome (Beyotime, China). The pathological changes of the neoplasms were observed using H&E staining. Neoplasm tissue sections were subjected to staining for 10 min, differentiation for 20 s, re-staining for 2 min, dehydration for 5 min, and permeabilization for 5 min, using hematoxylin staining solution (Component A), hydrochloric acid-ethanol, eosin staining solution (Component B), ethanol, and xylene, respectively. Positive rates of Ki-67, CD31 and CD44 in neoplasm tissues were observed using IHC and IF staining. Neoplasm tissue sections were subjected to antigen repair for 25 min, permeabilization for 10 min, and closure for 1 h using citrate buffer, 0.25% Triton X-100, and 5% sheep serum, respectively. Neoplasm tissue sections were incubated with Anti-Ki67 rabbit mAb, Anti-CD31 rabbit pAb, Anti-CD44 rabbit mAb, and Biotinylated Goat Anti-Rabbit IgG. Antibody information for the target protein is provided in Table S2. After all tissues were sealed, neoplasm tissue sections were photographed and scanned using a BX53 microscope (Olympus, Japan) and a VM1000 digital scanner (Motic, China).

QUANTIFICATION AND STATISTICAL ANALYSIS

All experiments were repeated at least three times and GraphPad Prism software (V9.0.0) was used to perform statistical analysis and visualization. Data between two and multiple groups were analyzed by STUDENT t-test/Mann-Whitney U-test and one-way ANOVA/Kruskal-Wallis test, respectively. $p < 0.05$ was considered statistically significant.

ADDITIONAL RESOURCES

Not Applicable.